$Y_{21}I_{18}C_{14}B_7$: Synthesis, Average Structure, and Structural Misfit

Oliver Oeckler, Viola Duppel, Hansjürgen Mattausch, and Arndt Simon*

Max-Planck-Institut für Festkörperforschung, Heisenbergstrasse 1, D-70569 Stuttgart, Germany

Received December 1, 1998

The new compound $Y_{21}I_{18}C_{14}B_7$ was prepared from YI_3, Y, C, and B at 1450 K. The average crystal structure was determined from single-crystal X-ray data. The structure consists of pseudoorthorhombic twisted metal atom double layers containing quasi-molecular CBC units. These are sandwiched by pseudohexagonal iodine layers. Owing to the symmetry and metric misfit the structure must be described with a large triclinic unit cell (space group $P\bar{1}$, $a = 10.660(2)$ Å, $b = 15.546(3)$ Å, $c = 18.416(3)$ Å, $\alpha = 82.49(2)°$, $\beta = 85.01(2)°$, $\gamma = 82.92(2)°$, $Z = 2$), which is probably only a good space-averaged approximation. Significant deviations from the averaged structure are indicated by unusual displacement parameters and the results of high-resolution electron microscopy.

Introduction

Borides and carbide borides of rare earth (Ln) metals exhibit a rich structural chemistry.[1,2] The borides are characterized by extended B−B bonding, and in carbide borides B−C bonding is also observed. Boron and carbon atoms form finite units of various length, one-dimensional zigzag chains, or two-dimensional networks. In rare earth metal boride carbide halides[3,4] the metal atom framework is formally fragmented by halogen atoms, and one-dimensional or quasi-molecular B_xC_y entities result. For example, BC, CBC, or CBBC units have been observed which can also be viewed as interstitial anions in cagelike voids of the Ln atom substructure. Boron atoms are always found in the center of trigonal Ln_6 prisms, and carbon atoms bonded to boron are usually located in distorted tetragonal pyramids which result from capping square faces of the Ln_6 prisms by additional Ln atoms. Therefore, most structures of rare earth metal boride carbide halides can be derived by "condensation" of a few characteristic building blocks. This is also true for the metal atom substructure of the title compound $Y_{21}I_{18}C_{14}B_7$. However, this is the first example of a rare earth metal halide with interstitial atoms where the halogen atom substructure does not meet perfectly the metrics and symmetry of the metal atom substructure and/or vice versa, the misfit leading to structural consequences. Here we report on the synthesis and structure of this compound.

Experimental Section

Synthesis. Yttrium metal (99.9%, Johnson Matthey, Karlsruhe) was hydrogenated at 970 K, crushed, and dehydrogenated under dynamical high vacuum ($<10^{-5}$ mbar) at 1070 K (Mo boat, 24 h). No hydrogen could be detected in the yttrium powder by the method described elsewhere.[5] YI_3 was prepared from Y metal and I_2 in evacuated silica tubes with slowly increasing temperatures from room temperature to 1000 K. The product was purified by distillation under high vacuum in Ta containers (three times). Boron (Aldrich, 99% with ca. 0.5% C) and graphite (Aldrich) were heated under dynamical high vacuum for approximately 2 days. $Y_{21}I_{18}C_{14}B_7$ was synthesized at 1450 K (3 weeks, then quenched in cold water) from stoichiometric mixtures of Y, YI_3, B, and C in Ta capsules sealed under Ar and enclosed in evacuated silica ampules. Usually the compound is obtained in the form of very small needles; sometimes larger crystals occur as flat needles. The starting materials as well as the product are sensitive against air and moisture, so all manipulations were performed with Schlenk techniques or in a drybox under purified argon.

Chemical Analysis. $Y_{21}I_{18}C_{14}B_7$ can be obtained in good yield (80−90% estimated from X-ray powder patterns and by optical microscopy). Traces of oxygen lead to the formation of impurities such as $Y_9I_8C_4O$[6] or $Y_7I_6C_3O$[7] (if the YI_3 is not well purified, the formation of $Y_{21}I_{18}C_{14}B_7$ is completely suppressed). The chemical composition of $Y_{21}I_{18}C_{14}B_7$ was obtained by structure determination and is confirmed in part by the preparation. In addition EDX analyses were performed with a JEOL JSM 6400 scanning electron microscope and a Philips CM30/ST transmission electron microscope. The Y:I ratios obtained from analyses on different crystals reach from 50:50 to 60:40, which is, within the expected deviation, in agreement with the value 54:46 calculated for $Y_{21}I_{18}C_{14}B_7$. No hydrogen could be detected[5] in the product.

X-ray Diffraction. Powder samples were characterized by a modified Guinier technique[8] (detection with imaging plates, Fuji BAS 5000) using capillaries. Histograms match with calculated patterns, although preferred orientation cannot be avoided. Extensive grinding easily leads to very diffuse patterns. Low-temperature powder patterns down to 19 K were obtained using the techniques described elsewhere.[9,10] No phase transitions could be detected.

Many crystals were checked for their quality by Laue and Buerger precession photographs. Only a few could be found showing sharp reflections up to angles of $2\theta \approx 40°$ (Mo Kα). For the best crystal found, data were collected on a one-circle diffractometer with an imaging plate area detector (Stoe IPDS) at 293(1) K using graphite-monochromated Mo Kα radiation. Some important crystallographic data are given in Table 1. The structure could be solved using direct methods.[11] However, the structure refinement[12] (based on F^2) is not very satisfying at first sight as the R indices are unusually large. This

(1) Wiitkar, F.; Kahlal, S.; Halet, J.-F.; Saillard, J.-Y.; Bauer, J.; Rogl, P. *J. Am. Chem. Soc.* **1994**, *116*, 251.
(2) Ansel, D.; Bauer, J.; Bonhomme, F.; Boucekkine, G.; Frapper, G.; Halet, H.-F.; Gougeon, P.; Saillard, J.-Y.; Zouchoune, B. *Angew. Chem.* **1996**, *108*, 2245; *Angew. Chem., Int. Ed. Engl.* **1996**, *35*, 2095.
(3) Mattausch, Hj.; Oeckler, O.; Simon, A. Submitted to *Inorg. Chim. Acta*.
(4) Mattausch, Hj.; Simon, A. *Angew. Chem.* **1995**, *107*, 1764; *Angew. Chem., Int. Ed. Engl.* **1995**, *34*, 1635.
(5) Eger, R.; Mattausch, Hj.; Simon, A. *Z. Naturforsch.* **1993**, *48b*, 48.
(6) Meyer, G.; Mattfeld, H.; Krämer, K. *Z. Anorg. Allg. Chem.* **1993**, *619*, 1384.
(7) Mattausch, Hj.; Borrmann, H.; Simon, A. *Z. Naturforsch.* **1993**, *48b*, 1828.
(8) Simon, A. *J. Appl. Crystallogr.* **1970**, *3*, 11.
(9) Simon, A. *J. Appl. Crystallogr.* **1971**, *4*, 138.
(10) Müller, R. Diplomarbeit, Universität Stuttgart, 1983.

10.1021/ic981377x CCC: $18.00
Published on Web 03/27/1999

Table 1. Crystallographic Data for $Y_{21}I_{18}C_{14}B_7$

fw	4395.12	
cryst syst	triclinic	
space group, Z	$P\bar{1}$, 2	
lattice parameters	$a = 10.660(2)$ Å	$\alpha = 82.49(2)°$
	$b = 15.546(3)$ Å	$\beta = 85.01(2)°$
	$c = 18.416(3)$ Å	$\gamma = 82.92(2)°$
vol	2994.9(9) Å^3	
temp	293 K	
calcd density	4.874 g/cm^3	
abs coeff	29.36 mm^{-1}	
R1, wR2 ($>2\sigma$)[a]	0.11, 0.28	

[a] $R1 = \sum||F_o| - |F_c||/\sum|F_o|$. $wR2 = \{\sum[w(F_o^2 - F_c^2)^2]/[w(F_o^2)^2]\}^{1/2}$, where $w = 1/[\sigma^2(F_o^2) + (0.1P)^2 + 80P]$ with $P = \mathrm{Max}(F_o^2) + (2F_c^2)/3$.

can be explained as due to a lack of perfect long-range ordering, as most high-order reflections ($2\theta > 40°$) can hardly be observed. In general, many reflections are very weak. Nevertheless, all boron and carbon atoms could be easily located from difference Fourier maps. The assignment of these atoms is fairly clear from their characteristic coordination and connectivity. The metal atom substructure containing B and C is well-known (although less distorted) from lanthanum carbide boride halides.[3] No significant difference Fourier peaks (indicating oxygen atoms) could be found in the tetrahedral interstices of the metal atom framework. The forty highest residual peaks are closer than 1.6 Å to either yttrium or iodine atoms. They indicate that the "thermal" ellipsoids, which show an unusually high degree of anisotropy, do not well model possible multiple split positions. A refinement with isotropic split positions for atoms with large displacement parameters leads to slightly better R values, but shall not be further discussed because the individual split positions cannot be refined anisotropically due to parameter correlation. To analyze whether the high anisotropy of the displacement parameters arises from thermal vibration, dynamical disorder, or static disorder a second data set was collected at 93(1) K. The equivalent isotropic displacement parameters become significantly smaller, but the anisotropy further increases. Hence, pronounced static disorder can be assumed, which is probably the main reason for the large R indices. No indications for a superstructure or twinning could be observed. However, diffuse X-ray scattering or a possible extremely weak superstructure might be hidden because of the moderate crystal quality. The refined atomic coordinates and selected interatomic distances are given in Tables 2 and 3, respectively.

Electron Diffraction and High-Resolution Electron Microscopy (HRTEM). Electron diffraction patterns and high-resolution images were taken with a Philips CM30/ST transmission electron microscope operated at 300 kV using a GATAN slow-scan CCD camera. The sample was introduced into the microscope using a transfer system designed for air-sensitive compounds.[13] Diffraction patterns were recorded for the [100] zone (approximately perpendicular to the layers of the structure) and the characteristic [711] zone to confirm the alignment of the crystallites by the tilting angles between the two positions. Observed patterns match well with patterns calculated on the basis of the results of the X-ray structure determination (cf. Figure 1). The calculated patterns (kinematical intensities) were produced with the program DIFPAT.[14] No superstructure reflections or diffuse scattering can be seen (with some crystals, weak diffuse rings were observed due to amorphous layers caused by hydrolysis of the air-sensitive crystals). High-resolution images were taken in [100] orientation, and simulated images were calculated from the X-ray positional parameters according to the multislice formalism.[15] The correct alignment of the zone axis for HRTEM images was checked by comparing the Fourier transformed images with diffraction patterns.

Table 2. Positional and Equivalent Isotropic Displacement Parameters for $Y_{21}I_{18}C_{14}B_7$

atom	x	y	z	U_{eq}[a]
I1	0.2871(2)	0.58695(12)	0.33366(11)	265(5)
I2	0.3601(2)	0.44985(13)	0.55703(11)	282(5)
I3	−0.3230(2)	0.14443(12)	0.73525(11)	279(5)
I4	0.3006(2)	0.73285(12)	0.48712(12)	294(5)
I5	0.3708(2)	0.32615(13)	0.78211(12)	284(5)
I6	0.3579(2)	0.59802(13)	0.71678(12)	298(5)
I7	−0.3316(2)	0.04608(13)	0.95340(12)	307(5)
I8	0.3159(2)	0.87327(14)	0.65310(14)	368(6)
I9	0.3617(2)	0.16859(12)	0.62293(12)	307(5)
I10	0.3521(2)	0.2934(2)	0.3999(2)	414(6)
I11	0.3447(3)	0.4911(2)	0.94494(13)	396(6)
I12	−0.3448(2)	−0.1259(2)	0.7926(2)	432(7)
I13	0.3338(3)	0.7605(2)	0.8818(2)	564(9)
I14	−0.3117(3)	0.3159(2)	0.89440(13)	494(8)
I15	−0.3482(3)	−0.2224(2)	1.0028(2)	593(9)
I16	0.3337(3)	0.0326(2)	0.8235(2)	626(10)
I17	−0.3426(3)	−0.0124(2)	0.5660(2)	684(11)
I18	0.3078(3)	0.4198(2)	0.1812(2)	564(9)
Y1	−0.1404(3)	−0.1205(2)	0.9164(2)	191(6)
Y2	−0.1355(3)	−0.0207(2)	0.7099(2)	230(7)
Y3	0.1166(3)	0.5728(2)	0.4964(2)	205(6)
Y4	0.1630(3)	0.2055(2)	0.7645(2)	228(7)
Y5	−0.1156(3)	0.1261(2)	0.8508(2)	241(7)
Y6	0.1226(3)	0.7156(2)	0.6429(2)	208(6)
Y7	0.1739(3)	0.4592(2)	0.6985(2)	222(7)
Y8	0.1695(3)	0.3156(2)	0.5569(2)	270(7)
Y9	0.1138(3)	0.9122(2)	0.4895(2)	246(7)
Y10	0.0917(3)	0.7698(2)	0.3492(2)	221(7)
Y11	0.1379(3)	1.0576(2)	0.6267(2)	273(7)
Y12	0.1570(3)	0.3544(2)	0.9102(2)	243(7)
Y13	0.1150(3)	0.8528(2)	0.7895(2)	264(7)
Y14	0.0840(3)	0.6312(2)	0.2076(2)	249(7)
Y15	0.1115(3)	0.4258(2)	0.3549(2)	225(7)
Y16	0.1077(3)	−0.2598(2)	0.9967(2)	267(7)
Y17	−0.1223(4)	0.0170(2)	1.0635(2)	322(8)
Y18	0.1468(3)	0.1712(2)	0.4232(2)	288(8)
Y19	0.1459(4)	0.6030(2)	0.8451(2)	337(9)
Y20	−0.1248(3)	−0.2742(2)	0.7813(2)	305(8)
Y21	0.1127(4)	0.4956(2)	1.0621(2)	443(11)
C1	0.062(2)	0.323(2)	0.6883(14)	120(50)
C2	−0.013(3)	−0.026(2)	0.835(2)	220(60)
C3	0.008(3)	0.109(2)	0.983(2)	200(60)
C4	0.025(3)	0.255(2)	0.871(2)	180(50)
C5	0.028(3)	0.323(2)	0.441(2)	220(60)
C6	0.016(4)	0.115(2)	0.730(2)	340(80)
C7	−0.039(3)	0.827(2)	0.453(2)	260(60)
C8	−0.025(3)	−0.171(2)	0.698(2)	290(70)
C9	0.032(3)	0.469(2)	0.585(2)	270(60)
C10	0.041(3)	0.471(2)	0.839(2)	290(70)
C11	0.023(3)	−0.385(2)	0.730(2)	190(60)
C12	−0.012(3)	0.969(2)	0.586(2)	260(60)
C13	−0.002(3)	−0.243(2)	0.876(2)	240(60)
C14	−0.004(5)	0.611(3)	0.988(3)	560(110)
B1	−0.020(3)	0.113(2)	0.366(2)	180(60)
B2	−0.052(4)	−0.174(2)	1.076(2)	240(70)
B3	−0.038(4)	0.673(2)	0.921(2)	310(80)
B4	−0.003(4)	0.256(2)	0.507(2)	260(70)
B5	−0.006(4)	−0.463(2)	0.775(2)	250(70)
B6	0.012(3)	0.394(2)	0.639(2)	200(60)
B7	0.038(4)	0.032(2)	0.776(2)	310(80)

[a] $\times 10^4$ Å^2; U_{eq} is defined as one-third of the trace of the orthogonalized $\mathbf{U}_{ij}$ tensor.

Results and Discussion

Average Structure. The structure of $Y_{21}I_{18}C_{14}B_7$ contains a metal atom substructure similar to those of $Ln_3X_2(CBC)$ (Ln = La, Ce; X = Cl, Br) and $Ln_9X_5(CBC)_3$ (Ln = La, Ce; X = Br,

(11) Sheldrick, G. M. *SHELXS, Program for the Solution of Crystal Structures*; Universität Göttingen: Göttingen, 1997.
(12) Sheldrick, G. M. *SHELXL, Program for the Refinement of Crystal Structures*; Universität Göttingen: Göttingen, 1997.
(13) Jeitschko, P. O.; Simon, A.; Ramlau, R.; Mattausch, Hj. *Eur. Microsc. Anal.* **1997**, *2*, 21.
(14) Skarnulis, A. J.; Liljestrand, G.; Kihlborg, L. *J. Chem. Soc., Chem. Commun.* **1979**, 1.
(15) Stadelmann, P. A. *Ultramicroscopy* **1987**, *21*, 131.

Table 3. Selected Interatomic Distances (Å) and Angles (deg) for $Y_{21}I_{18}C_{14}B_7$[a]

I1−Y14	3.262(4)	I15−Y1	3.088(4)	Y10−Y11	3.448(5)
I1−Y15	3.272(4)	I15−Y12	3.100(4)	Y10−Y14	3.605(5)
I1−Y10	3.340(4)	I16−Y17	3.033(4)	Y12−Y14	3.473(5)
I1−Y3	3.363(4)	I16−Y4	3.176(4)	Y12−Y21	3.517(5)
I2−Y8	3.088(4)	I17−Y18	3.028(4)	Y12−Y21′	3.740(5)
I2−Y7	3.143(4)	I17−Y9	3.083(4)	Y12−Y16	3.548(5)
I2−Y3	3.219(4)	I17−Y2	3.574(5)	Y12−Y19	3.884(4)
I3−Y2	3.113(4)	I18−Y20	3.139(4)	Y13−Y20	3.441(5)
I3−Y10	3.143(4)	I18−Y21	3.169(5)	Y13−Y17	3.598(5)
I3−Y5	3.162(4)			Y14−Y21	3.591(5)
I4−Y9	3.223(4)	Y1−Y13	3.452(4)	Y15−Y20	3.642(5)
I4−Y6	3.298(4)	Y1−Y17	3.466(5)	Y16−Y19	3.695(5)
I4−Y3	3.331(4)	Y1−Y16	3.507(4)	Y16−Y21	3.831(4)
I4−Y10	3.468(4)	Y1−Y20	3.649(5)	Y16−Y17	3.811(4)
I5−Y7	3.117(3)	Y1−Y17	3.693(5)	Y17−Y17	3.385(8)
I5−Y4	3.136(4)	Y1−Y5	3.901(4)	Y19−Y20	3.464(5)
I5−Y12	3.169(4)	Y2−Y13	3.433(4)	Y19−Y21	3.522(6)
I6−Y19	3.127(4)	Y2−Y11	3.455(5)	Y21−Y21	3.437(9)
I6−Y7	3.157(4)	Y2−Y18	3.621(5)		
I6−Y6	3.209(4)	Y3−Y8	3.471(4)	C1−B6	1.42(4)
I7−Y17	3.097(4)	Y3−Y15	3.502(4)	C2−B7	1.43(4)
I7−Y5	3.124(4)	Y3−Y3	3.546(6)	C3−B2	1.47(4)
I7−Y1	3.200(4)	Y3−Y15	3.691(4)	C4−B2	1.50(4)
I8−Y13	3.166(4)	Y4−Y14	3.478(4)	C5−B4	1.54(4)
I8−Y11	3.242(4)	Y4−Y10	3.526(4)	C6−B7	1.45(5)
I8−Y6	3.424(4)	Y4−Y5	3.527(5)	C7−B4	1.43(4)
I9−Y8	3.074(4)	Y4−Y11	3.688(4)	C8−B1	1.46(4)
I9−Y11	3.102(4)	Y4−Y12	3.757(4)	C9−B6	1.45(4)
I9−Y4	3.278(4)	Y5−Y17	3.502(5)	C10−B5	1.54(4)
I10−Y18	3.038(4)	Y5−Y16	3.718(5)	C11−B5	1.42(4)
I10−Y15	3.181(4)	Y6−Y18	3.410(4)	C12−B1	1.47(4)
I10−Y8	3.374(4)	Y6−Y20	3.509(5)	C13−B3	1.54(4)
I11−Y19	3.135(4)	Y6−Y15	3.518(4)	C14−B3	1.50(5)
I11−Y21	3.138(5)	Y6−Y13	3.643(5)		
I11−Y12	3.249(4)	Y7−Y14	3.467(4)		
I12−Y20	3.093(4)	Y7−Y15	3.484(4)	C8−B1−C1	145(3)
I12−Y2	3.103(4)	Y7−Y8	3.655(5)	C3−B2−C4	150(3)
I12−Y1	3.304(4)	Y8−Y10	3.461(5)	C14−B3−C13	142(4)
I13−Y16	3.085(4)	Y8−Y18	3.583(5)	C7−B4−C5	145(3)
I13−Y13	3.101(4)	Y9−Y18	3.398(5)	C11−B5−C10	143(3)
I13−Y19	3.513(5)	Y9−Y9	3.459(6)	C1−B6−C9	149(3)
I14−Y16	3.057(4)	Y9−Y11	3.524(4)	C2−B7−C6	146(4)
I14−Y14	3.064(4)	Y9−Y11′	3.648(5)		
I14−Y5	3.540(5)	Y9−Y10	3.655(4)		

[a] For I−I distances cf. Figure 4.

I);[3] however, the geometry is slightly different. Metal atom double layers containing CBC units are sandwiched by iodine atom layers on both sides as shown in Figure 2. The metal atom sheets consist of two $3^34^2 + 3^6$ nets stacked upon each other. These sheets are twisted, whereas they are more or less flat in $Ln_3X_2(CBC)$ and undulated in $Ln_9X_5(CBC)_3$, respectively. They can also be described as condensed $Y_8(CBC)$ units consisting of bicapped boron centered trigonal Y_6 prisms with carbon atoms located in the caps and bonded to the boron atom. The symmetry of the $(Y_3CBC)_n$ layers is pseudoorthorhombic. The iodine atoms form pseudohexagonal layers in a very distorted close-packed arrangement. Due to the symmetry and metric misfit the structure must be described with a large triclinic unit cell (see Figure 3). The CBC groups are nonlinear with angles of about 146(4)° (mean of 7 independent CBC groups) and C−B distances of about 1.47(5) Å (mean of 14 independent distances). For the CBC units in $La_9Br_5(CBC)_3$ approximately the same values have been determined.[16] For the latter compound a formal charge distribution $(La^{3+})_9(Br^-)_5[(CBC)^{7-}]_3{\cdot}e^-$ seems to be reasonable, whereas for $Y_{21}I_{18}C_{14}B_7$ the stoichiometry does not allow all anions to be $(CBC)^{7-}$ and I^-. However, the CBC angle

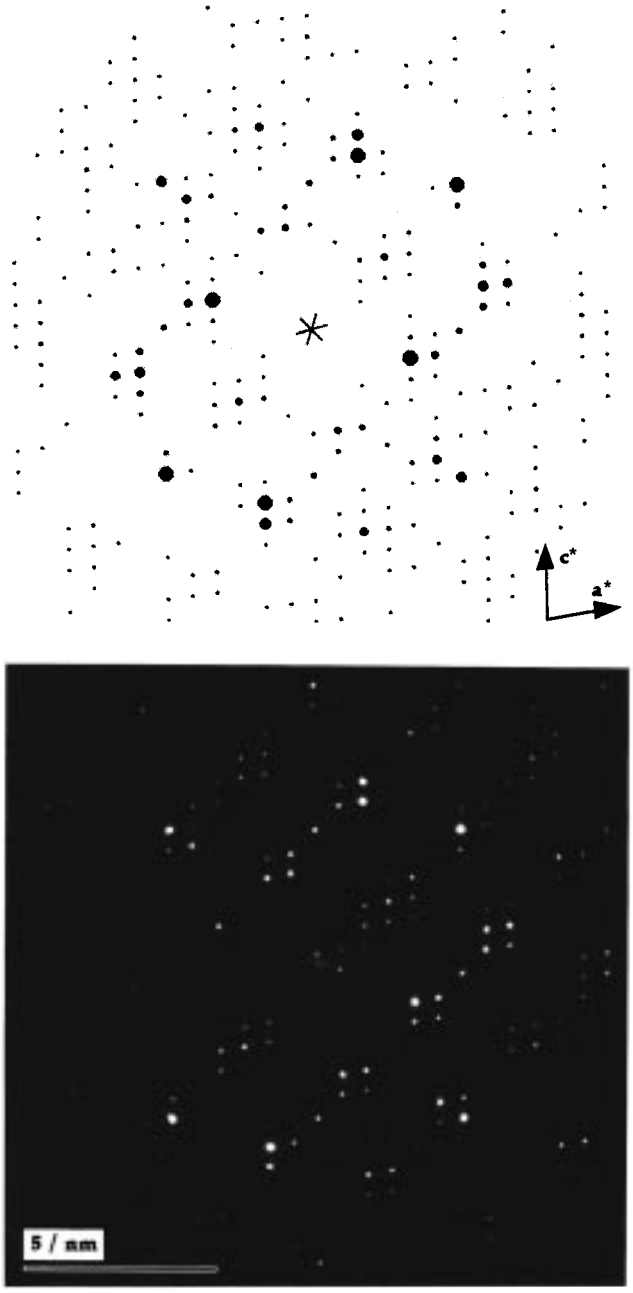

Figure 1. Electron diffraction pattern (SAD), zone axis [100]; experimental (bottom) and calculated on the basis of X-ray data (top).

in $La_9Br_5(CBC)_3$ is between what one could expect for $(CBC)^{5-}$ (isoelectronic with CO_2, linear) and $(CBC)^{7-}$ (isoelectronic with SO_2, about 120°). The question arises whether the enlarged angle of $(CBC)^{7-}$ is associated with some degree of cation−anion back-bonding. On the other hand, it has been shown for C_3^{4-} (isoelectronic with $(CBC)^{5-}$) that the bending angle is not very characteristic for the electronic structure of these quasi-molecules, as packing effects in the crystal strongly influence the bending.[17] Relatively small deviations from an "ideal" geometry are only associated with minor changes in the orbital energies. From this point of view, the most reasonable charge distribution seems to be $(Y^{3+})_{21}(I^-)_{18}[(CBC)^{5-}]_7{\cdot}10e^-$, which assumes 10 electrons per formula unit (about 0.5 per Y atom) delocalized in Y d states, but this is not consistent with measurements of the electrical conductivity. Sintered powder

(16) Mattausch, Hj.; Simon, A.; Felser, C.; Dronskowski, R. *Angew. Chem.* **1996**, *108*, 1805; *Angew. Chem., Int. Ed. Engl.* **1996**, *35*, 1685.

(17) Hoffmann, R.; Meyer, H.-J. *Z. Anorg. Allg. Chem.* **1992**, *607*, 57.

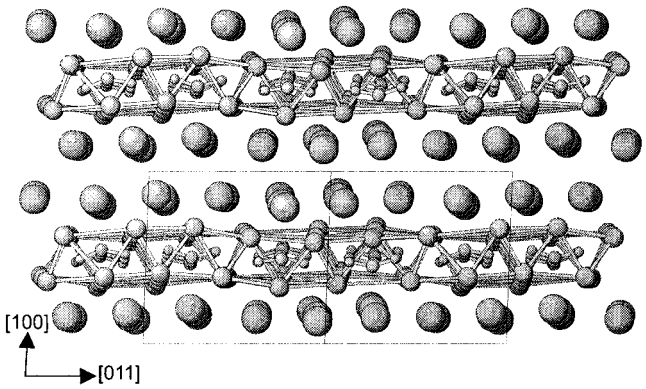

Figure 2. Projection of the structure of $Y_{21}I_{18}C_{14}B_7$ along [011]. I, Y, C, and B are shown as spheres with decreasing radii.

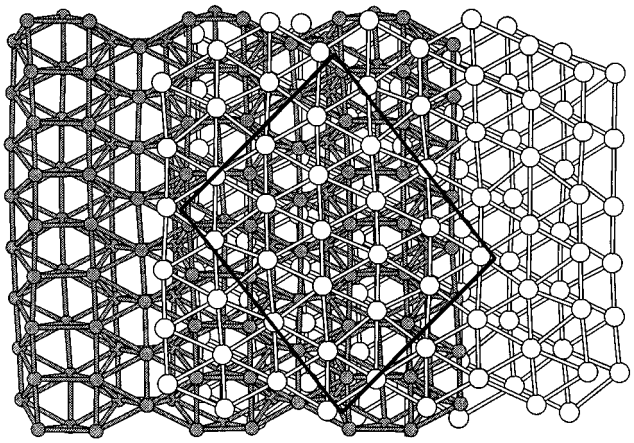

Figure 3. Projection of the structure of $Y_{21}I_{18}C_{14}B_7$ along [100] (I, white; Y, gray; B and C are not drawn). The metal atom double layer and the iodine atoms are omitted toward the right and the left, respectively.

pellets are found to be semiconducting (with a 0.05 eV band gap calculated from the temperature dependence of the resistivity) although the impurities are metallic (except traces of YOI). This might be due to preferred orientation of the crystallites, as the conductivity can be expected to be more or less two-dimensional, but could also be explained assuming a certain degree of nonstoichiometry. Only 0.25 electrons per Y atom are missing in order to assume nonlinear $(CBC)^{7-}$ entities. The charge balance could easily be adjusted by slightly varying interstitials (for example, if some carbon atoms were missing, BC groups with lower charge would result). But in general it must be emphasized that the picture of quasi-molecular entities as interstitials is only a simplified approach which cannot be expected to explain details of the electronic structure.

Structural Misfit. The obvious misfit between metal and halogen atom layers leads to a high degree of distortion in both substructures. Nevertheless some of the halogen atoms covering the metal atom sheets are not located in suitable depressions of the latter, but more or less above lines connecting neighboring Y atoms. The distances between those pairs of Y atoms are significantly larger than between others where no halogen atom takes such a position. On the other hand, only the iodine atoms not situated in depressions of the Y atom layer show unusal anisotropy of the displacement parameters. It is reasonable to assume that they shift toward the neighboring depressions to some extent; in other words, they occupy split positions. This obviously influences the distortion of the iodine atom layer: I−I distances are longest in the directions of the largest axes of the ellipsoids, i.e., in the directions where displacement occurs

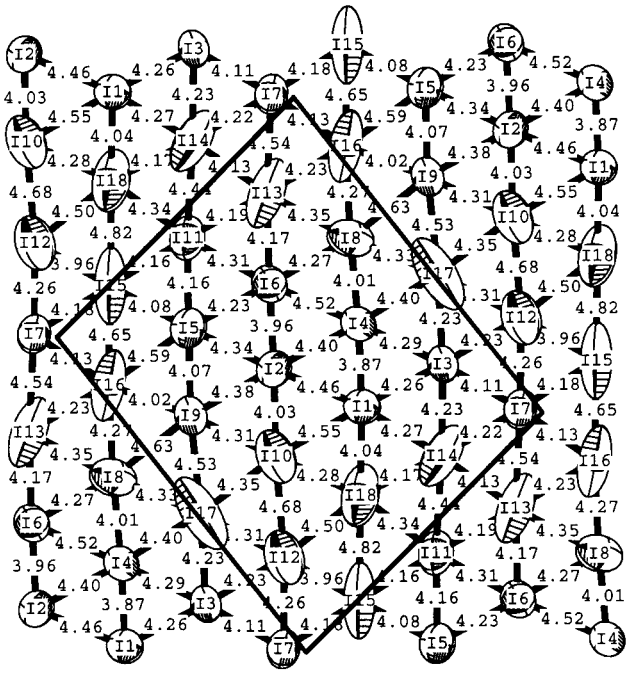

Figure 4. Plot of displacement ellipsoids for one layer of iodine atoms with interatomic distances (Å) indicated (esd's < 0.01 Å), same orientation as in Figure 3.

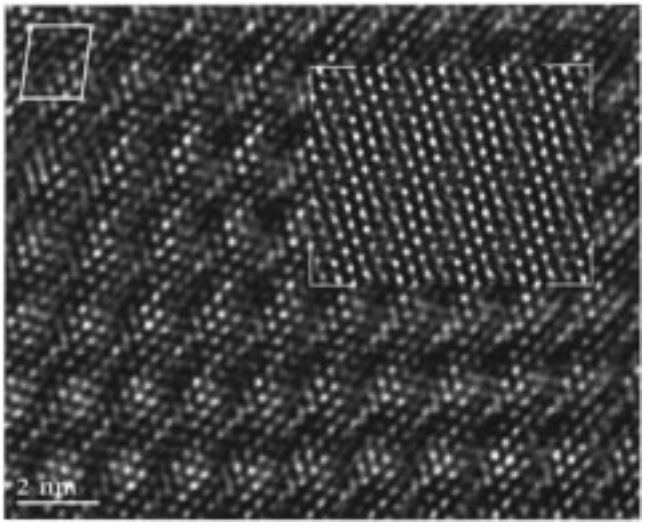

Figure 5. HRTEM image of $Y_{21}I_{18}C_{14}B_7$, zone axis [100]; inset: simulation (thickness 2 unit cells, defocus $\Delta f = -30$ nm); unit-cell dimensions are indicated.

predominantly (cf. Figure 4). A similar disorder can be discussed for the yttrium atom layers, although it is less pronounced there. Owing to the bonding to CBC units the metal atom double layers are obviously more rigid than the iodine atom layers. As no superstructure or diffuse scattering could be observed with both X-rays and electrons, no long-range correlation in the disorder is ascertainable. Apparently the disorder is static, as it does not decrease at low temperatures and does not give rise to phase transitions down to 19 K. HRTEM images provide additional information; however, they cannot explain exactly how displacements change from one unit cell to the other. In principle, HRTEM images for the [100] zone axis (Figure 5) match with simulated images. Yet, the observed patterns show a much less homogeneous intensity distribution than the simulations on the basis of the averaged structure. This could be explained in terms of the iodine atoms shifting toward depressions, creating larger

ones in other places. For areas larger than a few unit cells HRTEM images show no ideal translational symmetry. For this reason, other simulations, e.g., with split positions, using the lattice parameters of the averaged structure cannot be expected to give a better fit. This can be due to irregular modulations in the sense of an intermediate-range correlation between atom shifts, but can also arise from "macroscopic" bending or undulation of the crystallites.[18] However, if bending or undulation of the crystallites is present, it is probably due to the misfit and would explain why no "good" single crystals could be found after numerous attempts. Although occasionally unusual displacement parameters are observed for halogen atoms in reduced rare earth halides with interstitials, usually the metal and nonmetal substructures adapt to each other almost perfectly, which seems to be impossible in $Y_{21}I_{18}C_{14}B_7$.

Acknowledgment. We thank Gisela Siegle for the conductivity measurements.

Supporting Information Available: Tables listing detailed crystallographic data, anisotropic displacement parameters, and more interatomic distances, an electron diffraction pattern ([711] zone), and an additional HRTEM image. This material is available free of charge via the Internet at http://pubs.acs.org.

IC981377X

(18) Bursill, L. A.; Pring, A.; Smith, D. J.; Shannon, M. D. *Philos. Mag.* **1982**, *B45*, 771.